20th Australasian Fluid Mechanics Conference
Perth, Australia
5-8 December 2016

Numerical study of haemodynamic changes in an idealised coronary artery with a partially embedded stent implanted

B. Jiang[1], E.K.W. Poon[1], P. Barlis[1,2], S.J. Illingworth[1] and A.S.H. Ooi[1]

[1]Department of Mechanical Engineering, Melbourne School of Engineering, The University of Melbourne, Victoria 3010, Australia
[2]North West Academic Centre, Melbourne Medical School, The University of Melbourne, Victoria 3010, Australia

Abstract

Incomplete stent apposition (ISA) is often found in patients with drug eluting stent implantation, and lack of neointimal coverage is considered as one of the underlying mechanisms leading to late stent thrombosis. In-vivo studies using intravascular optical coherence tomography (OCT) showed that stents implanted at locations with complex arterial geometry can lead to struts embedded into the artery on one side, but malapposed on the other side. In this study, we carried out three dimensional computational fluid dynamics studies on a partially embedded coronary stent. Stent struts are partially embedded in portion of the circular artery's circumference and malaposed elsewhere. Maximum malapposition distances (MD) used in this study are 0.255 mm (moderate) and 0.555 mm (severe). Time-averaged wall shear stress (TAWSS) is used as the haemodynamic metric to evaluate the clinical significance of ISA. TAWSS decreases along the circumferential direction as MD decreases from the maximum ISA side to the embedded side. Case with severe ISA has larger area of high TAWSS on the arterial wall at the proximal end and low TAWSS at the distal end of the stent. Area percentage of very high TAWSS (> 5 Pa) on stent surface of severe ISA case is significantly larger than moderate ISA case (35% *versus* 6%), which may result in higher chance of stent thrombosis.

Introduction

Coronary artery disease, caused by accumulation of atherosclerotic plaques and thus a stenosed artery, is one of the leading causes of death in the world [1]. Percutaneous coronary intervention (PCI) with stents has been a common treatment for stenosis [2]. Over the past decades, continuous research efforts have been made to improve coronary stent design and its mechanical properties, in terms of improving haemodynamics performance. One notable area in coronary stent design is the use of novel materials with superior properties, from bare metal stent (BMS) to drug eluting stent (DES) and the latest bioresorbable vascular scaffolds (BVS) [3]. In addition, stent apposition, that allows fast endothelial coverage, is also important for the best clinical outcome. However, incomplete stent apposition (ISA) remains common when stents are deployed at complex lesions, especially with DES in the follow up diagnosed by images obtained using optical coherence tomography (OCT) [4]. OCT images in many studies show that malapposed stent struts usually appear on one side of the lumen [5]. ISA is considered to be a major factor in the development of complications after stenting, such as in-stent restenosis and/or stent thrombosis (ST), possibly due to both low wall shear stress (WSS) and high platelets activating shear rates in the vicinity of the malapposed stent struts [3].

WSS is a commonly used metric to evaluate the haemodynamic changes [3,4]. Studies have shown that low WSS (commonly accepted cut-off is less than 0.5 Pa) is prone to neointimal thickening and linked to atherosclerosis [8]. There is significant negative correlation between level of plaque deposition and WSS [9]. Endothelial cells are WSS sensors, high WSS (> 3 Pa) has been implicated in expansive remodelling of vessels and also atherosclerotic plaque destabilization [10]. Platelet activation under high shear rate (> 1000/s, equavlent to WSS > 2.5 Pa) at the surface of malapposed stent struts is linked to thrombotic phenomena [3]. We aim to provide in-depth understanding of the haemodynamic behaviour of a partially malapposed stent with different maximum malapposition distance (MD). The resultant WSS distributions may elucidate regions of abnormal endothelium responses that ultimately result in adverse clinical outcomes such as restenosis and stent thrombosis.

Method

Computational Fluid Dynamics (CFD) modelling was applied to investigate the pulsatile blood flow in an idealised coronary artery with a generic stent. The artery was assumed to be a rigid circular tube with a constant diameter of 3 mm [11] and 38.8 mm in length (see figure 1). A coronary stent, that composed of 10 stent hoops with a total length of 18.8 mm was placed in the middle of the circular artery model [12]. Each stent hoop had 10 crown elements and stent strut was 90 μm thick. A realistic stent model allows detailed analysis of the WSS patterns such as variations of WSS in the circumferential direction. A realistic stent model also has a longer circumferential length than a simplified model due to its sinusoidal pattern. As a result, a simplidied stent model might underestimate the low WSS area distal to the stent hoop. Stent struts were considered to be 50% embedded at the bottom of circular artery (Figure 1), and malapposition distance increased gradually in the circumferential direction with a maximum at the top. We considered two maximum malapposition distances: 0.255 and 0.555 mm as moderate and severe ISA, respectively [3]. We employed a pulsatile inlet velocity boundary condition to minic the changes in coronary flow over a cardiac cycle [7,12–15]. Pulsatile flow in a stented coronary arteries can introduce both marco [16] and mirco recirculation environments [17] that cannot be observed using steady velocity inlet. A zero pressure boundary condition was used for the outlet. The arterial wall and the stent surface were set to be rigid and non-slip. CFD was performed in the resting condition with a heartbeat rate of 75 beats/min (i.e. a pulsatile period of T = 0.8 s), and the mean volume flow rate was 1.3 ml/s. Blood was assumed to be Newtonian with a density of ρ = 1000 kg/m^3, and dynamic viscosity of μ = 2.5×10^{-3} Pa·s. The corresponding Reynolds numbers (based on artery diameter (D) and instantaneous velocity (U), $\mathrm{Re_D} = \rho \cdot U \cdot D/\mu$) varied, from 107 to 342 throughout the cardiac cycle and Womersley number ($\alpha = (D/2) \cdot (\rho \cdot 2\pi \cdot T/\mu)^{0.5}$) was ~2.66. Numerical results from the last cycle were analysed to ensure that all transients have been convected out of the simulation domain.

Mesh was generated using ICEM-CFD (ANSYS INC., Canonsburg, PA, USA) which has about 46 million tetrahedral cells for the moderate malapposed case and 47 million for the

severely malapposed case. Maximum cell size around the stent struts was set to be 0.01 mm and maximum cell sizes on the arterial wall, inlet and the outlet were all set to be 0.1 mm. CFD simulations were carried out by directly solving the incompressible Navier–Stokes equations using an open source CFD software OpenFOAM-2.1.1 (OpenCFD Ltd., ESI group, Bracknell, UK).

In order to understand the haemodynamic changes, well established metrics time averaged wall shear stress (TAWSS), that has shown to be strongly linked to atherogenesis and thrombogenesis [13], is employed.

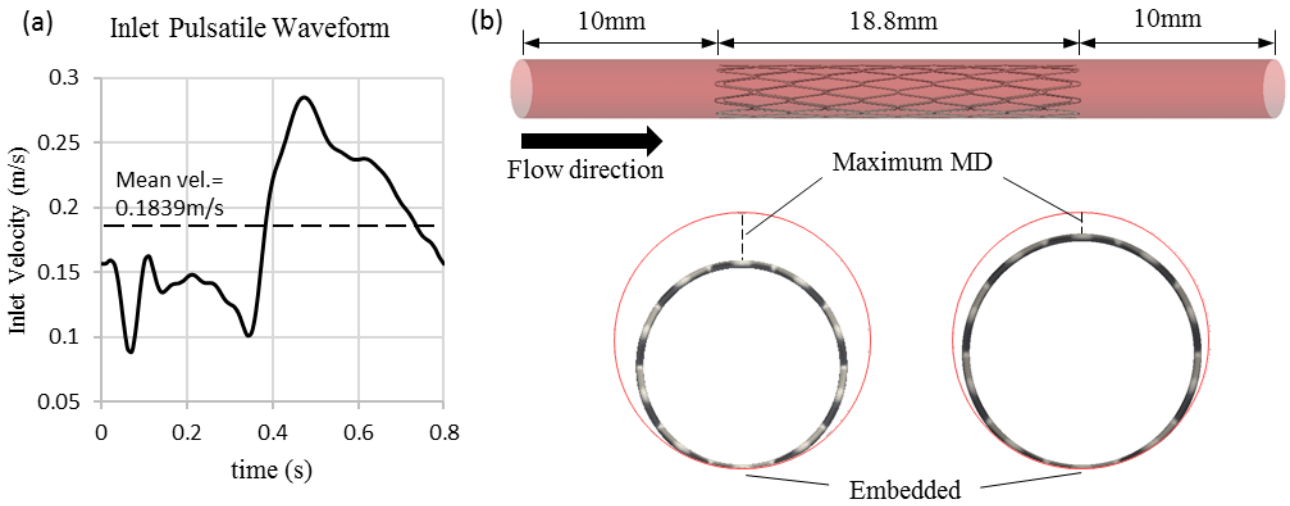

Figure 1 (a) inlet pulsatile velocity waveform. (b) side view and cross-sectional view of stent location in the artery and illustration of maximum malapposition distance at the top side of the artery.

Results and discussion

Comparison of TAWSS on Arterial Wall

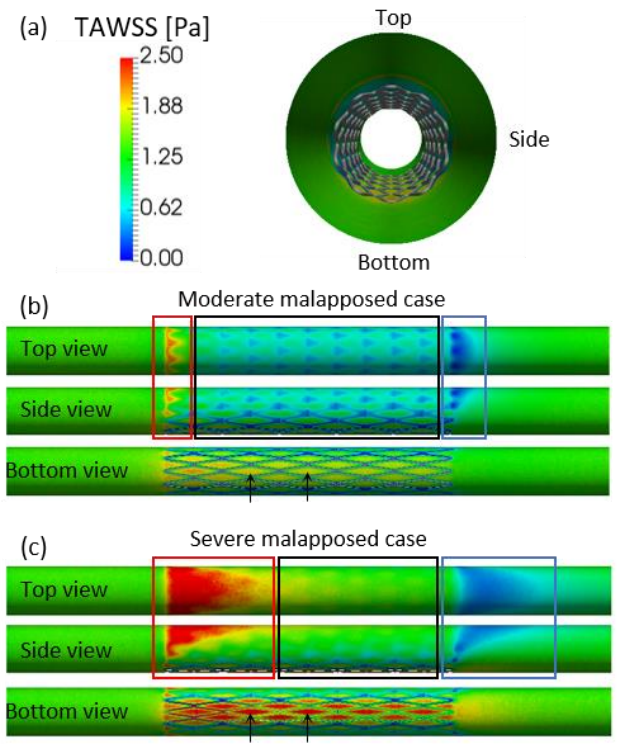

Figure 2 Time-averaged wall shear stress (TAWSS) result comparison of the moderate and severe malapposed cases. (a) definition of the location top, side and bottom; (b) TAWSS from the three views of the moderate malapposed case; (c) TAWSS from the three views of the severe malapposed case.

Figure 2 shows the results of time-average wall shear stress (TAWSS) on the arterial wall. In the stented segment, there is an overall decrease of TAWSS along the streamwise direction. TAWSS is also reduced from top to side in circumferential direction as MD decreases. Both moderate and severe cases had a sudden TAWSS increase at the proximal end of the stent and a sharp decrease at the distal end as shown in the red and blue boxes. However, at the bottom, in areas bounded by the stent struts (some of them are indicated by the black arrows), percentage of high TAWSS area became higher than the top and the side regions. With the presence of the malapposed stent, blood flow between the stent and the arterial wall is limited due to the merging boundary layer from the lumen and strut surface. Meanwhile, this has resulted in a higher flow velocity on the embedded side than the unstented region. In the moderate MD case, figure 2 (b), blood has to squeeze through a significantly narrower space between the stent struts and the arterial wall, resulting in a lower velocity due to a stronger effect of the merging boundary layers from the lumen and strut surface, and therefore relatively lower TAWSS is observed in the middle section of the stented region (black box) than the severe MD case. At the top and the side of the model (in the black box), where stent struts were relatively far away from the arterial wall, TAWSS decreased slightly along the longitudinal direction (fluctuating from 0.4 to 0.9 Pa) as influenced by the stent struts. In the side view of figure 2 (b), at the lower part of the black box, the MD is so small that the low TAWSS region mimics the shape of the stent struts. This effect was not that obvious in the severe malapposed case. In the severe malapposed case, figure 2 (c) the area of high TAWSS and low TAWSS (in the blue and red boxes) were both substantially larger than the corresponding area of the moderate malapposed case.

Figure 3 shows the cross-sectional time-averaged blood flow velocity magnitude contour at different longitudinal locations within the stented region. These four locations were 10, 16, 22, and 28.3 mm from the inlet. In the moderate MD case, The wall-normal velocity gradient generally decreases from location (a) to (d). Also at location (b), (c) and (d), velocity gradient gradually increased from the maximum malapposed side to the embedded side, whereas velocity gradient at location (a) varied very little throughout the circumference. The severe malapposed case gives rise to a higher velocity gradient at the wall (indicated in the boxes)

compared to the corresponding areas in the moderate malapposed case, except at location (d). In the severe case, velocity increased over a significant longer distance normal to the arterial wall at the top (indicated in the boxes) from (a) to (d), which means that velocity gradient decreases, while the decreasing rate of velocity gradient at the side of the cross-sections was much smaller.

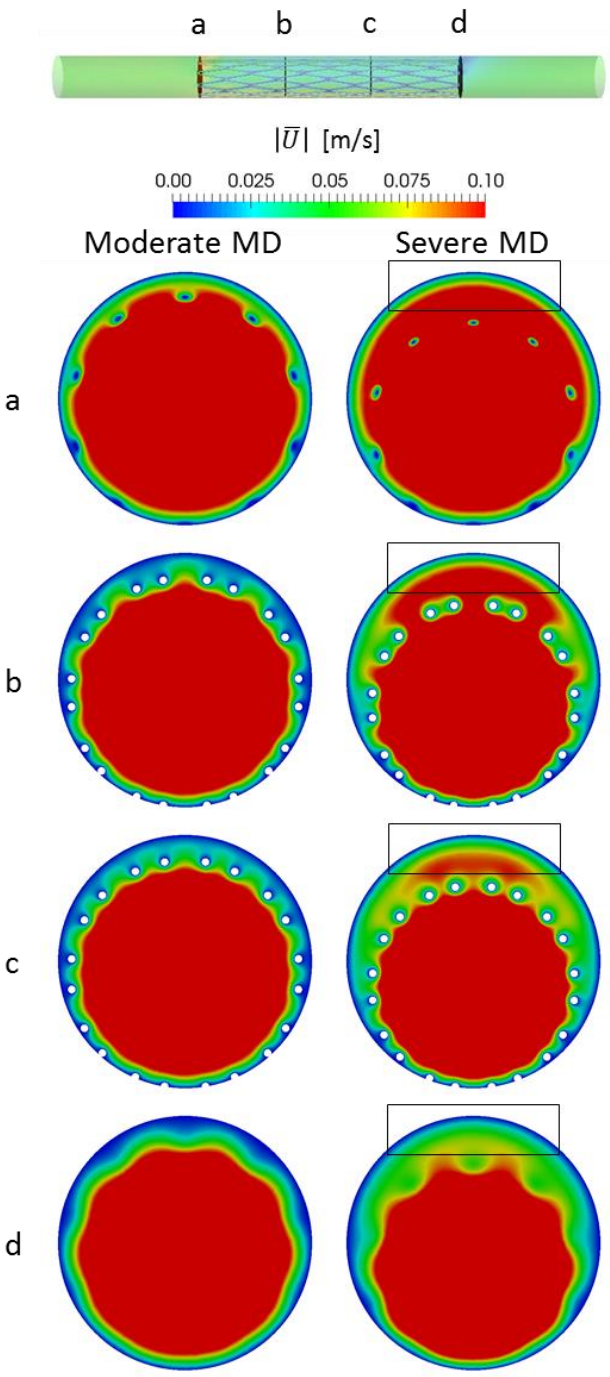

Figure 3 $|\overline{U}|$ contours in cross-sections at different locations of the two cases.

TAWSS on Stent Surface

High shear rate has been shown to directly correlate with platelet activation which leads to thrombus generation and shear rate over 1000/s is considered to be undesirable [3]. In our in-silico setup, shear rate over 1000/s corresponds to a wall shear stress of 2.5 Pa. TAWSS on the surface of malapposed stent struts were much higher than that on the arterial wall as they were closer to the center of the artery and encountered a higher local blood flow velocity.

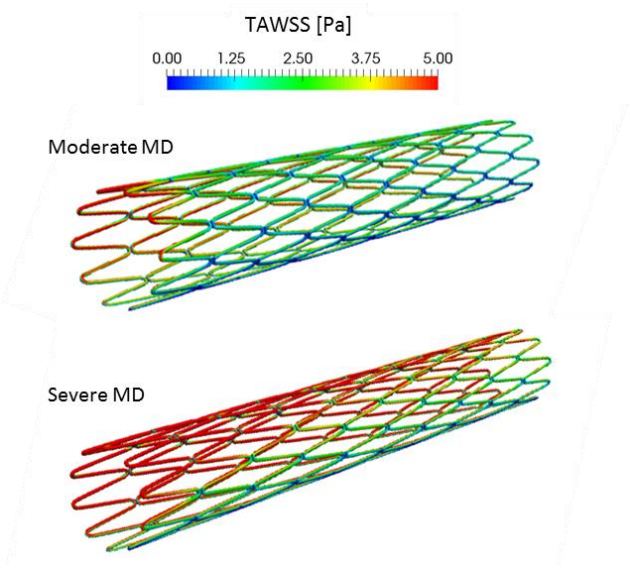

Figure 4 TAWSS distribution on stent struts of moderate MD and severe MD cases.

As shown in Figure 4, for both cases, highest TAWSS appeared on the top region at the proximal end of the stent. TAWSS gradually decreases along the streamwise direction and also decreases along the circumferential direction as MD decreases from the top to the bottom of the artery. TAWSS on stent struts of the moderate MD case was considerably lower than that on the severe MD case (2.53 *verus* 4.07 Pa in average TAWSS over the total stent surface). The area percentage of each threshold of TAWSS on the stent struts of both cases are compared in Figure 5. In the moderate MD case, acceptable TAWSS (< 2.5 Pa) was about 52.9% of the whole stent surface, and the percentage decreased damatically for each range of higher TAWSS thresholds. For the highest range (> 7.5 Pa), the area percentage of the moderate MD case was almost negligible. For the severe MD case, higher TAWSS (> 2.5 Pa) took the major proportion of stent surface (72.6%). From the threshold of 5 Pa onwards, the severe MD case had about 5 times of undesirable area percentage of the moderate MD case. Therefore, larger MD gives a much higher chance of platelet activation.

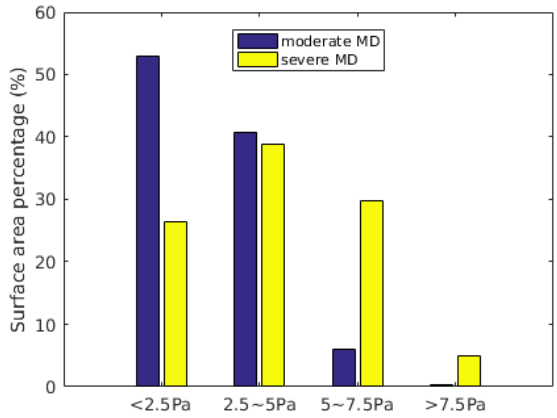

Figure 5 Percentage of areas comparison of certain TAWSS on stent struts.

Conclusions

Stent implantation often leads to the straightening of the artery at the stented segament [18]. Therefore we simplified the model using a straight lumen which can reveal the fundamental physics of ISA. In addition, the employment of complex stent model and pulsatile flow, despite the increase of computational requirement, are essential to show complicated coronary flow patterns and

fluctuations in WSS circumferentially in a stented artery. We performed high fidelity CFD simulations to systematically investigate partially malapposed stent in the circumferential direction. Two maximum malapposition distance (MD = 0.255 and 0.555 mm) were considered. Maximum malapposition distance was set to be at the top of the artery. This region always experiences a high TAWSS at the proximal end of the stented region, and a low TAWSS area distal to the stent. In general, TAWSS magnitude was higher in the severely malapposed case, but the lower TAWSS region distal to the stent was also much larger than the moderate MD case. In the longitudinal direction, both moderate and severe MD cases had decreasing TAWSS, however this phenomenon was more significant in the severe MD case. In the circumferential direction, TAWSS decreases from the maximum malapposition distance side to the embedded side but this effect was less obvious in the relatively small MD case. TAWSS on the stent surface was also undesirably high in the severe MD case. 72.6% of the stent area was over 2.5 Pa, while the moderate MD case had only 47.1% above that threshold. Overall severely malapposed stent is prone to have slower or no neointimal coverage and higher chance of stent thrombosis.

Acknowledgement

This work was supported by the ARC Linkage Project (LP150100233) and VLSCI high performance computing grant (VR0210).

References

[1] WHO 2014 *Global status report on noncommunicable diseases 2014*

[2] Foin N, Lee R D, Torii R, Guitierrez-Chico J L, Mattesini A, Nijjer S, Sen S, Petraco R, Davies J E, Di Mario C, Joner M, Virmani R and Wong P 2014 Impact of stent strut design in metallic stents and biodegradable scaffolds *Int. J. Cardiol.* **177** 800–8

[3] Foin N, Gutiérrez-Chico J L, Nakatani S, Torii R, Bourantas C V., Sen S, Nijjer S, Petraco R, Kousera C, Ghione M, Onuma Y, Garcia-Garcia H M, Francis D P, Wong P, Di Mario C, Davies J E and Serruys P W 2014 Incomplete stent apposition causes high shear flow disturbances and delay in neointimal coverage as a function of strut to wall detachment distance implications for the management of incomplete stent apposition *Circ. Cardiovasc. Interv.* **7** 180–9

[4] Ozaki Y, Okumura M, Ismail T F, Naruse H, Hattori K, Kan S, Ishikawa M, Kawai T, Takagi Y, Ishii J, Prati F and Serruys P W 2010 The fate of incomplete stent apposition with drug-eluting stents: an optical coherence tomography-based natural history study *Eur. Heart J.* **31** 1470–6

[5] Attizzani G F, Capodanno D, Ohno Y and Tamburino C 2014 Mechanisms, Pathophysiology, and Clinical Aspects of Incomplete Stent Apposition *J. Am. Coll. Cardiol.* **63** 1355–67

[6] Harper E M, Palmer T J and Alphey J R 1997 Wall Shear Stress Temporal Gradient and Anastomotic Intimal Hyperplasia *Geol. Mag.* **134** 403–7

[7] Poon E K W, Barlis P, Moore S, Pan W-H, Liu Y, Ye Y, Xue Y, Zhu S J and Ooi A S H 2014 Numerical investigations of the haemodynamic changes associated with stent malapposition in an idealised coronary artery *J. Biomech.* **47** 2843–51

[8] Malek A M, Alper S L, Izumo S, AM M, SL A and S I 1999 Hemodynamic shear stress and its role in atherosclerosis *JAMA* **282** 2035–42

[9] Jiang Y, Kohara K and Hiwada K 1999 Low wall shear stress contributes to atherosclerosis of the carotid artery in hypertensive patients. *Hypertens. Res.* **22** 203–7

[10] Dolan J M, Kolega J and Meng H 2013 High wall shear stress and spatial gradients in vascular pathology: A review *Ann. Biomed. Eng.* **41** 1411–27

[11] Dodge J T, Brown B G, Bolson E L and Dodge H T 1992 Lumen diameter of normal human coronary arteries. Influence of age, sex, anatomic variation, and left ventricular hypertrophy or dilation. *Circulation* **86** 232–46

[12] Gundert T J, Dholakia R J, McMahon D and LaDisa J F 2013 Computational Fluid Dynamics Evaluation of Equivalency in Hemodynamic Alterations Between Driver, Integrity, and Similar Stents Implanted Into an Idealized Coronary Artery *J. Med. Device.* **7** 11004

[13] Beier S, Ormiston J, Webster M, Cater J, Norris S, Medrano-Gracia P, Young A and Cowan B 2016 Hemodynamics in Idealized Stented Coronary Arteries: Important Stent Design Considerations *Ann. Biomed. Eng.* **44** 315–29

[14] LaDisa J F, Olson L E, Douglas H a, Warltier D C, Kersten J R and Pagel P S 2006 Alterations in regional vascular geometry produced by theoretical stent implantation influence distributions of wall shear stress: analysis of a curved coronary artery using 3D computational fluid dynamics modeling. *Biomed. Eng. Online* **5** 40

[15] Rajamohan D, Banerjee R K, Back L H, Ibrahim A a and Jog M a 2006 Developing pulsatile flow in a deployed coronary stent. *J. Biomech. Eng.* **128** 347–59

[16] van Wyk S, Wittberg L P, Bulusu K V., Fuchs L and Plesniak M W 2015 Non-Newtonian perspectives on pulsatile blood-analog flows in a 180° Curved artery model *Phys. Fluids* **27** 0–28

[17] Tenekecioglu E, Poon E K W, Collet C, Thondapu V, Torii R, Bourantas C V, Zeng Y, Onuma Y, Ooi A S H, Serruys P W and Barlis P 2016 The Nidus for Possible Thrombus FormationInsight From the Microenvironment of Bioresorbable Vascular Scaffold *JACC Cardiovasc. Interv.* **9** 2167–8

[18] Wentzel J J, M. Whelan D, Van Der Giessen W J, Van Beusekom H M M, Andhyiswara I, Serruys P W, Slager C J and Krams R 2000 Coronary stent implantation changes 3-D vessel geometry and 3-D shear stress distribution *J. Biomech.* **33** 1287–95